2023 IEEE International Conference on Robotics and Automation (ICRA 2023)
May 29 - June 2, 2023. London, UK

A Hybrid Steerable Robot with Magnetic Wrist for Minimally Invasive Epilepsy Surgery

Changyan He, Robert H. Nguyen, Cameron Forbrigger, James Drake, Thomas Looi, Eric Diller

***Abstract*— Dexterity is demanded for an endoscopic tool to handle complicated procedures in neurosurgery, e.g., removing diseased tissue from inside the deep brain along a tortuous path. Current robotic tools are either rigid or lack wristed motion ability at the tip, leading to limited usage in minimally invasive procedures. In this paper, a hybrid steerable robot with a magnetic wristed forceps is proposed to provide enhanced dexterity for endoscopic epilepsy surgery. A set of three precurved Nitinol tubes with concentric deployment, called a concentric tube robot (CTR), serves as a 6 degrees-of-freedom (DoF) robotic positioner. The magnetic wristed forceps is composed of a rotational wrist joint, and forceps at the tip, both of which are actuated remotely by magnetic fields. The magnetic wrist and forceps provide an extra rotational DoF and a gripping DoF on top of the CTR, respectively. The magnetic wrist and gripper are designed to have a hollow channel along their common axis, inside which a soft tube is deployed as a second functional tool for irrigation or suction. An electromagnetic navigation system (eMNS) with 8 coils is used to create the quasi-static magnetic fields. Experimental characterization of the robot kinematics is performed and the results show the mean motion error of CTR is 2.8 mm. The workspace is also analyzed and results indicate that the proposed hybrid robot has a significantly larger reachable area compared to the one of the CTR alone. Mock epilepsy procedures are performed on a brain phantom to validate the feasibility of the hybrid robot for neurosurgery applications.**

I. Introduction

Epilepsy, affecting 1% of the pediatric population, approximately 50–70 million people worldwide, is a chronic non-communicable disease of the brain and is characterized by patients experiencing seizures. The seizures, as a result of hyperactivity by various neuronal clusters, are brief episodes of alterations in awareness that may be focal, involving sensations or motor movements, or with loss of consciousness and bowel or bladder control. Patients with epilepsy are experiencing recurrent seizures throughout their life, and therefore, have severely impacted life quality and are at significantly increased risk of premature death. Simple tasks such as driving a vehicle or walking on the street become challenges for them. Although antiepileptic drugs (AEDs) are the primary form of treatment to release the seizures, approximately one-third of epilepsy patients have seizures that are unresponsive to pharmacologic therapy [1]. For these patients, epilepsy surgery has been shown as a cost effective method to stop the seizure activity by typically localizing and isolating the seizure zones in the brain with resection and/or disconnection operations. However, it remains as a high risk procedure because the vast majority of operations are performed open and require prolonged intensive and post-operative care.

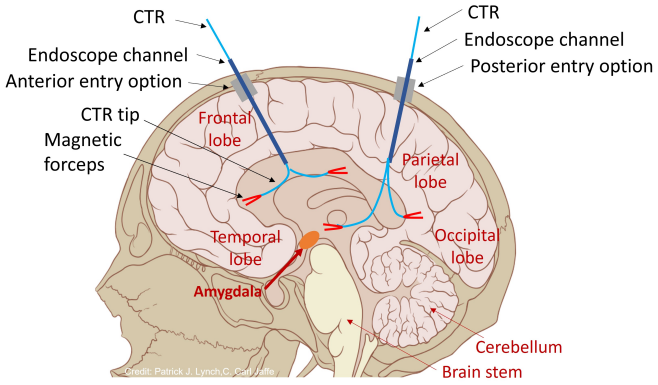

Fig. 1: Minimally invasive neurosurgery assisted by the hybrid steerable robotic tool.

To improve surgical outcomes and shorten patient recovery, robotic assistance and endoscopy has been introduced to neurosurgery to perform the procedures with a minimally invasive (MI) approach, as illustrated in Fig. 1. Endoscopy can reduce the invasiveness by eliminating the need for large craniotomies and reducing the volume of healthy brain tissue that must be disrupted to access the surgical site [2], while robotic assistance can provide accurate navigation and precise localization [3].

Early research about robot-assisted neurosurgery can be traced back to the late 1980s with a primary focus on integration of preoperative imaging [4]. With the advancements of robotic technologies, many modern robotic systems have been developed, which can be generally categorized into three groups: a) rigid robotic tool, b) the da Vinci surgical system adapted tool, c) micro-catheter, and d) continuum robotic tool.

Rigid robotic tools focus more on stereotactic neurosurgery compared to the tools in the other two categories. A rigid endoscopy tool is typically mounted at a robot arm's end and MRI or other image modalities are used to navigate the tool to reach the diseased tissue [5]–[8]. Since the tool is rigid, the tool's passing path inside the brain is constrained to be straight, otherwise, rotational/tilting motions of the tool inevitably apply pressure to surrounding delicate brain tissue, which may cause potential damage [9].

The da Vinci surgical system has been widely accepted in many abdominal procedures and deployed in more than 5000 hospitals over the world. It offers "wrist-like" capability

*This work was supported by CIHR Project Grant 452287.

C. He, R.H. Nguyen, J. Drake, and T. Looi are with PCIGITI lab in the Hospital for Sick Children.

C. He, C. Forbrigger and E. Diller are with the Microrobotics lab in University of Toronto. (email: changyan.he@utoronto.ca)

at the tooltip to enable the surgeon to perform dexterous operation through one or multiple key holes. [10] reports the feasibility and safety of employing the daVinci surgical system to perform key-hole neurosurgery. However, due to the bulky size, the instrument could not be advanced to the deep cisterns without significant clashing, which limits its application in neurosurgery.

The micro-catheter, as an emerging technology, has also been investigated for neurosurgery. It is typically made out of elastomers and actuated either by magnetic field [11], [12] or fluid flow [13]. A micro-catheter can be steered into a highly tortuous pathway due to its low stiffness. However, the soft body in turn results in micro-catheters being limited to neurovascular applications since it can not deliver any practical manipulative forces to target tissue.

Continuum shape based robotic tools have been recently proposed to provide dexterous manipulation, sufficient stiffness, and compact tool size. The concentric tube robot (CTR) is one of the prominent continuum designs that has been largely investigated for neurosurgical procedures [14], [15]. The CTR is a needle-sized flexible robot composed of a set of nested superelastic and precurved tubes that are typically made out of Nitinol (NiTi). By a heat treatment process, the NiTi tube can be preset to a given curvature and retain its shape in free space. After assembly, each elastic tube can be independently translated and rotated with respect to one another, then a tentacle-like motion can be achieved [16], [17]. However, the existing CTRs are lacking wristed manipulation similar to the da Vinci surgical system at its tip. This limitation reduces the robot tip's reachability and precludes the robot from carrying out complicated procedures, e.g., amydalohippocamectomy, a critical procedure of epilepsy. More than that, a CTR typically needs to mount a cable-driven end-effector at its tip to perform cutting or grasping operations. The actuation of the end-effector applies external forces/torques on the CTR's tip, which in turn causes unstable deflections along the CTR length due to the NiTi tubes' elasticity.

In this paper, we propose a magnetically controlled hybrid steerable robot for performing minimally invasive epilepsy surgery. The hybrid robot integrates a 6 DoF CTR with a 2 DoF magnetically actuated end-effector with a wrist and forceps (referred as magnetic wristed forceps), as shown in Fig. 2. The wrist provides additional dexterity for the CTR tip and endows the robot with "wrist-like" capability for tissue manipulation. The surgeon is able to insert and deploy the hybrid steerable robot into specific seizure areas and use the magnetic forceps to cut and isolate the target areas.

For the first time, we propose a magnetically actuated wristed steerable robot for neurosurgery. Using an external magnetic field to directly actuate the tips of the instruments avoids the complexity of pulley transmissions, which are commonly adopted in other wristed robotic tools [10]. It also allows the tips to be controlled precisely with sufficient force. Our previous work has shown that magnetic forceps can generate necessary gripping force in neurosurgery [18]. Concentric tubes for positioning the tool tips are remarkably

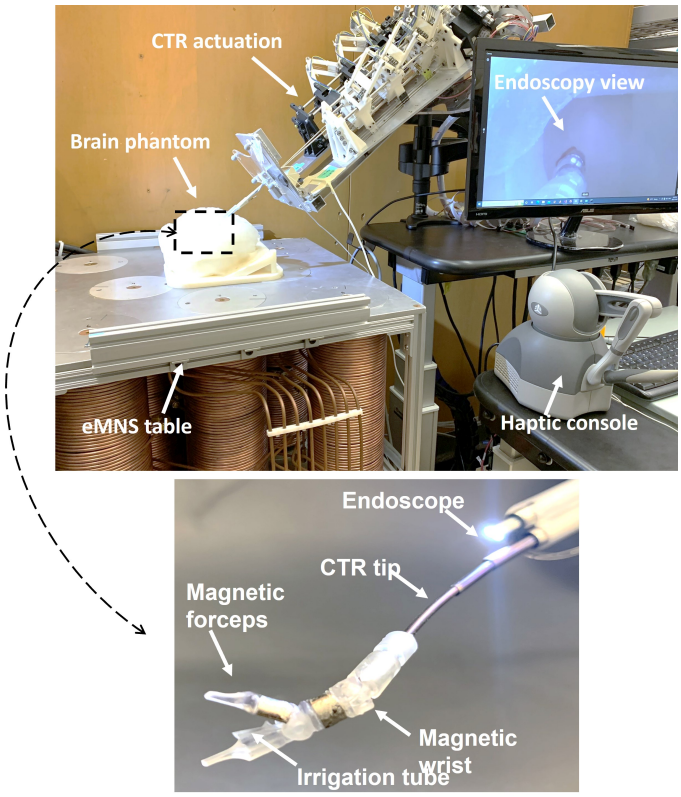

Fig. 2: Overview of the hybrid steerable robot. The system includes a magnetic end-effector with a wrist and forceps, a CTR positioner, a haptic console, an eMNS, and an endoscopy sub-system. An irrigation tube is deployed in the hollow channel of the magnetic end-effector and the CTR.

dexterous and strong at this scale, and are controlled by simple remote motors that either advance or rotate the tips to achieve a large workspace. We also contend that ultimately these simpler magnetic tools could be manufactured and assembled inexpensively and be disposable. This would lead to a new generation of minimally invasive surgical tools for epilepsy and other neurosurgical indications.

II. Design and Modelling

The proposed hybrid steerable robot consists of two main components, a CTR and magnetically actuated wristed forceps. The wristed forceps are mounted at the tip of the CTR. The design and modelling of the CTR and the wristed forceps are described in this section. The hybrid robot is controlled under a human-in-the-loop control strategy, in which the CTR and magnetic forceps both are maneuvered by the human operator using a haptic device. The image captured by the endoscope is displayed on a monitor to provide visual feedback.

A. Concentric tube robot

1) Design: The CTR is designed to actuate three precurved NiTi tubes with rotation and advancement motions. An overview of the CTR's mechanics is shown in Fig. 3 (a). The tubes are nested in a telescoping configuration and each tube is carried by a cart separately, i.e., three carts are utilized in total. The carts are installed and hung in parallel

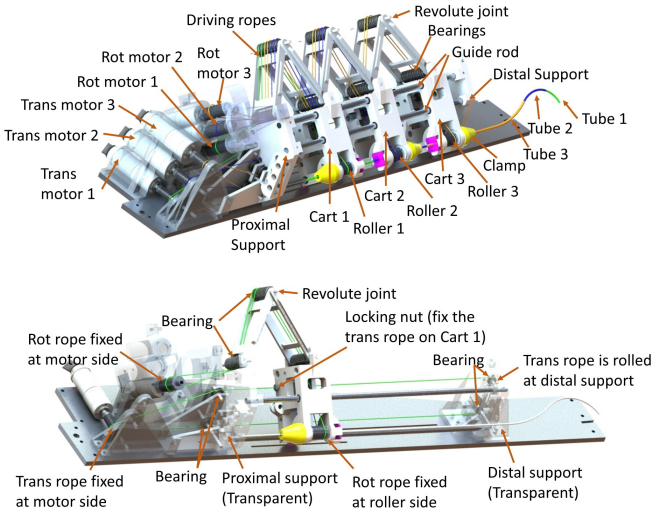

Fig. 3: Design of CTR robot. (a) The three NiTi tubes, denoted as tube 1 for inner tube, tube 2 for middle tube, and tube 3 for outer tube, are carried by three carts separately. Three sets of ropes are wound from the motors to the carts and used to actuate the tubes with rotation and advancement motions. Tubes 1,2,3 and rope sets 1,2,3 are differentiated by the color green, blue, and yellow, respectively; (b) Mechanism of a single cart. The cart is hung at two guide rods and driven by two sets of ropes.

on two guide rods that are fixed by a proximal support and a distal support. Each cart is driven by two sets of ropes to rotate and advance the NiTi tube, respectively. The ropes and motors that are used for rotary actuation are denoted as "rot rope" and "rot motor", and the ones for advancement actuation are denoted as "trans rope" and "trans motor". A rot rope starts winding from a rot motor's axis to a cart's roller by passing over the top of a/multiple movable bridge(s), and continues winding back to the same rot motor. The rot motor can then transmit bidirectional pull torques to the cart roller and further rotate the NiTi tube that is inserted through and secured on the roller. A trans rope starts winding from a trans motor's axis to the distal support by passing through a cart frame, and continues winding back to the same trans motor. The rope is locked to the cart frame by a stopper, such that the trans motor can apply bidirectional drag forces on the cart, which further advances the NiTi tube, as shown in Fig. 3 (b). We adopt the pulley transmission instead of screw-nut or gear transmission that are commonly used in other CTR systems, to reduce friction and compact actuation unit.

2) Modelling: Among many state-of-the-art modelling methods for CTRs [19], the geometry-based model [20] is adopted in this paper for its closed form solution. For completeness, the modelling procedures are briefly outlined below.

Assuming negligible external forces and torsional rigidity of the tubes, the forward kinematics can be formulated as a series of transformations between successive constant-curvature segments starting at the tip of the trocar and ending at the distal end of the CTR. The forward kinematics, i.e., the mapping from tube parameters, including rotary angles θ and advancement lengths l, to the tip pose can be resolved

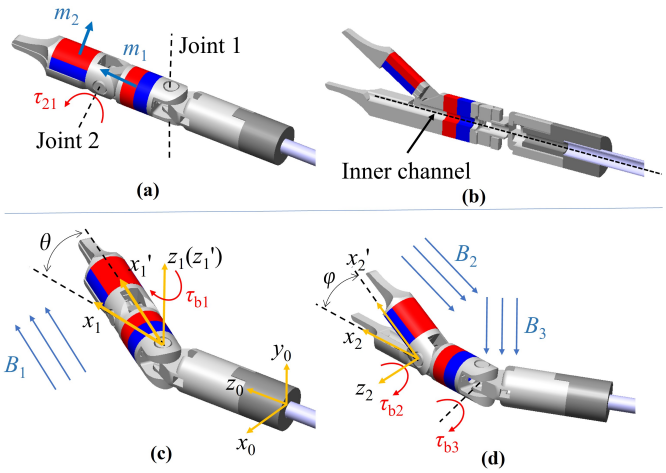

Fig. 4: Design of the magnetic wristed forceps. (a) Overall structure. (b) Section view showing that the magnetic wristed forceps has an inner channel. (c) External magnetic field B_1 is applied to actuate the wrist to rotate. (d) External magnetic field B_2 and B_3 is applied to open the forceps.

as the transformation:

$$T(\theta,l) = E(\kappa_{x1},\kappa_{y1},s_1)\cdots E(\kappa_{xn},\kappa_{yn},s_n), \tag{1}$$

where n is the number of constant-curvature segments, s_i is the length of segment i, and κ_{xi} and κ_{yi} are the x and y components of the resultant curvature of segment i, respectively. The transformation E for each segment is

$$E(\kappa_x,\kappa_y,s) = \begin{bmatrix} \frac{\kappa_x^2+\kappa_y^2\cos(s||\kappa||)}{||\kappa||^2} & \frac{\kappa_x\kappa_y(1-\cos(s||\kappa||))}{||\kappa||^2} & \frac{\sin(s||\kappa||)\kappa_y}{||\kappa||} & \frac{\kappa_y(1-\cos(s||\kappa||))}{||\kappa||^2} \\ \frac{\kappa_x\kappa_y(1-\cos(s||\kappa||))}{||\kappa||^2} & \frac{\kappa_y^2+\kappa_x^2\cos(s||\kappa||)}{||\kappa||^2} & -\frac{\sin(s||\kappa||)\kappa_x}{||\kappa||} & -\frac{\kappa_x(1-\cos(s||\kappa||))}{||\kappa||^2} \\ -\frac{\sin(s||\kappa||)\kappa_y}{||\kappa||} & \frac{\sin(s||\kappa||)\kappa_x}{||\kappa||} & \cos(s||\kappa||) & \frac{\sin(s||\kappa||))}{||\kappa||} \\ 0 & 0 & 0 & 1 \end{bmatrix} \tag{2}$$

and the resultant curvature κ for a set of p overlapping tubes is

$$\kappa = \left(\sum_{i=1}^{p} K_i\right)^{-1} \sum_{i=1}^{p} K_i\bar{\kappa}_i, \tag{3}$$

where $K_i = E_iI_i$ is the stiffness matrix for tube i, with E_i and I_i being the modulus of elasticity and cross section moment of inertia of tube i, respectively, and $\bar{\kappa}_i$ is the curvature of tube i prior to assembly.

The inverse kinematics, i.e., the mapping from spatial tip positions/velocities to tube input curves that are associated with tube parameters, can be resolved using a pseudo-inverse solution based on Eq. 1.

B. Magnetic wristed forceps

1) Design: We propose a serial link magnetic end-effector, as shown in Fig. 4, which includes a wrist (joint 1) and forceps (joint 2). A cylindrical NdFeB magnet is employed as the wrist link and its moment m_1 is aligned toward the forceps tip. A half cylindrical NdFeB magnet is used as the forceps link with the moment m_2 directed upward. The rest of the components, including joint couplers and

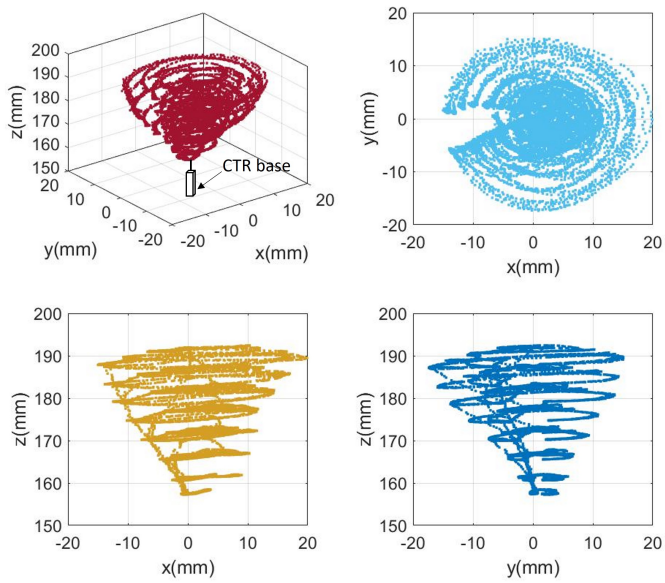

Fig. 5: CTR workspace analysis.

forceps jaws are all 3D printed with resin. The end-effecter is designed to have a hollow channel from the proximal end all the way to the forceps tip along its main axis, as shown in Fig. 4 (b), which can be used for housing an additional surgical instrument, e.g., an irrigation/suction tube or a laser fiber. Due to the perpendicular moment directions of the wrist magnet and forceps magnet, the interactive magnetic torque τ_{21} keeps the forceps closed at rest. When an external field B_1 is applied over the workspace, as shown Fig. 4 (c), the magnet m_1 is subjected to the magnetic torque τ_{b1}, which actuates the wrist to rotate. While an external magnetic field B_2 with its main direction toward the forceps proximal end is applied over the workspace, the torque τ_{b2} is generated to open the forceps, as shown in 4 (d). The magnetic wristed forceps can be installed on the tip of CTR using a 3D printed adapter.

2) Modelling: The external field B_1 applies a torque on magnet m_1, which can be expressed as:

$$\tau_{b1} = m_1 \times B_1 \tag{4}$$

This torque τ_{b1} actuates the wrist to rotate and eventually align the axis of magnet m_1 to the projected direction of field B_1 onto the local x_1y_1 plane, since the angle $< \vec{m}_1, \vec{B}_{1xy} >$ becomes zero and the torque τ_1 is minimized at that position. It should be noted that the joints are assembled with transition fit so the friction is negligible ideally. The wrist angle θ can be obtained by resolving the angle between field B_1 and the initial direction of $\vec{x}_1$, i.e., $\theta = < \vec{x}_1, \vec{B}_{1xy} >$. Given the simple serial joints, the tip position of the forceps in base frame $\{0\}$ can be written as:

$$(p_x,\ p_y,\ p_z) = (l_2 \sin\theta,\ 0,\ l_1 + l_2 \cos\theta). \tag{5}$$

An external field B_2 that is generated in the opposite direction of $\vec{x}_2$ applies a torque on magnet m_2, which is expressed as $\tau_{b2} = m_2 \times B_2$. The torque τ_{b2} then opens the forceps as a binary action. An additional field B_3 is generated along the wrist axis and applied for the magnet m_1 to create a "secure" torque τ_3 to hold the wrist with its instant position by increasing the friction at joint 1.

TABLE I: CTR parameters (Unit: mm, N/mm^2)

	Curve length	Curve radius	OD	ID	Elastic modulus
Tube 1	20	55.7	1.48	1.30	34500
Tube 2	20	69.7	1.97	1.88	34500
Tube 3	40	81.0	2.45	2.30	34500

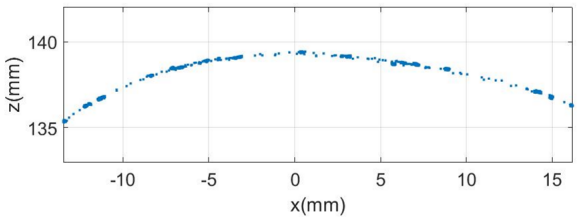

Fig. 6: Magnetic wristed forceps workspace result. The tip position of the magnetic forceps is measured under the actuation of the field.

III. Kinematic Performance

The kinematic performance for the hybrid robot is experimentally analyzed in this section, including motion accuracy evaluation and workspace characterization, to show the robot feasibility for micro-procedures.

A. Concentric tube robot

The geometrical and mechanical parameters of each tube are listed in Table I. Six DC servo motors (Maxon, Switzerland) are employed as actuators and a PC-based controller (Beckhoff Automation, USA) is used as the low-level PD controller. An electromagnetic tracking system (Aurora, NDI, Canada) is utilized to track and record the tip position of the CTR in real time.

The workspace of the CTR is obtained as the shape of an inverted bell with the bottom diameter of 32 mm and height of 35 mm, as shown in Fig. 5 (a), which covers the major area of the third ventricle of a human brain and thus is sufficient for performing epilepsy procedures.

The motion accuracy is also analyzed by commanding the CTR to reach a set of 16 target locations and comparing the measured tip positions to the target positions. The evaluation was repeated for 5 times and the results indicate the mean absolute error of tip positioning is 2.8 mm with a standard deviation 1.5 mm.

B. Magnetic wristed forceps

The magnets that are used to prototype the wristed forceps are off-the-shelf products (SM Magnetics, USA). The wrist magnet has the shape of a cylinder with OD, ID, and height of 4mm, 1mm, and 3mm, respectively. The forceps magnet has the shape of a half cylinder with OD, ID, and height of 4mm, 1mm, and 4mm, respectively. Both magnets are made of NdFeB (Grade N45).

A previously developed electromagnetic navigation system (eMNS) [21] is used as field source to generate a magnetic field around the hybrid robot tip, as shown in Fig. 2. The

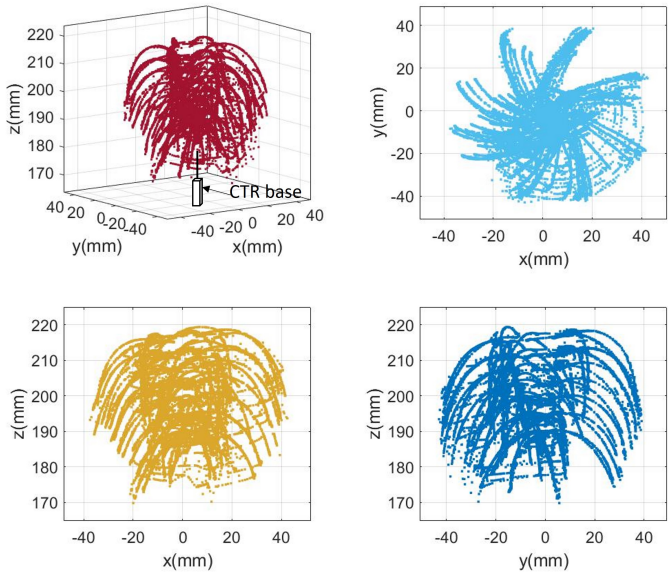

Fig. 7: Hybrid robot workspace.

eMNS is composed of eight electromagnetic coils and the coils are deployed in parallel to provide a large and open workspace and facilitate surgical operations. The eMNS can generate up to a 45 mT field.

The workspace of the magnetic wristed forceps is evaluated under the field actuation. An optical tracking system (Polaris Spectra, NDI, Canada) is used to capture and localize the tip position of the forceps by mounting a tracking ball at its tip. The results, as shown in Fig. 6, indicate that the workspace can span over 54°. Due to the friction of wrist joint and non-uniform field of the eMNS, open-loop control for the wrist angle would lead to considerable error. Therefore the human-in-loop control architecture is utilized to increase the wrist localization accuracy by involving the operator's active feedback and motion compensation.

Binary closing/opening forceps jaws is also tested 20 times and the results indicate the forceps open/close status can be controlled with a 80% success rate.

C. Hybrid robot

The magnetic wristed forceps is installed at the tip of the CTR , as shown in Fig. 2. The optical tracking system is used to characterize the reachable workspace of the hybrid robot by mounting a tracking ball at the forceps' tip. The results is shown in Fig. 7 and suggest that the magnetic wristed forceps significantly increases the CTR's reachability and expands the workspace to a "fireworks" shape with a rim diameter of 80 mm. The minimum curvature radius (corresponding to maximum deflection) that the hybrid robot can reach is 32.4 mm, which is 14% less than the one of the CTR alone (38.1 mm). Besides, the maximum curvature length of the hybrid robot is extended 1.5 times larger to 54.9 mm from the one of the CTR (35.5 mm).

IV. Experiments and Results

A. Control architecture

A tele-operation control architecture is implemented for maneuvering the hybrid robot by using a 6 DoF haptic device (Geomagic Touch, 3D Systems, USA) as the master console. The human operator is expected to hold and manipulate the stylet to send Cartesian position commands to the CTR controller and the eMNS. The eMNS then generate appropriate field to rotate the magnetic wrist. The opening of the magnetic forceps is controlled by a press-button on the stylet.

B. Dexterity performance

Pilot experiments are carried out to evaluate the dexterity of the hybrid robot by steering the robotic tip to pass through a set of three rings, as shown in Fig. 8 and the supporting video. The three rings are installed on three bars and deployed in the robot's workspace with a preset configuration. The hybrid robot is manually controlled with the haptic console to perform the pass task. The procedure is repeated 5 times with 100% success rate.

C. Mock epilepsy procedures

A brain phantom is used to perform the mimic epilepsy procedure, which is fabricated based on our existing set of neuro-endosocopy training models and modified to include the corpus callosum and hippocampus [22]. The composite brain phantom is placed on the skull base and fixed in place. A piece of raspberry is placed at the channel of the hippocampus to mimic the amygdala and serves as the target tissue to be removed.

A soft silicone tube is inserted through the hollow channel of the CTR and magnetic wristed forceps and its end is placed at the middle of the forceps acting as an irrigation tool. The other end of the silicone tube is connected to a pump to access the flushing fluid.

The experiment is aimed to reach and pick out the mock amygdala with the hybrid robot. An engineer who is familiar with the robotic system is invited to practice on the phantom to become familiar with the model. The experiment procedures are shown in Fig. 8 and the supporting video. The successful picking rate is analyzed to be 80%.

V. Discussion and Conclusion

The misalignment and pulley transmission of the CTR actuation contribute to the CTR's kinematic error. Currently we use open loop control with human operator's feedback as the control method, which relies on operator's concentration and instant action to achieve accurate robot localization. In the future, feedback control with endoscopy image will be investigated to provide an "easy" control architecture for operators.

The forceps opening field B_2 is applied at the opposite direction of the wrist magnet m_1, which would possibly apply a undesired torque for m_1 and sharply turn the wrist to its limit angle if B_2 is not fully inversely aligned with m_1. Although we apply a "secure" field B_3 to increase the friction of the wrist joint and hold the wrist at its instant position, the failure chance reaches 20% based on the experiment evaluation. However, this control instability can be eliminated by changing the dipole direction of the

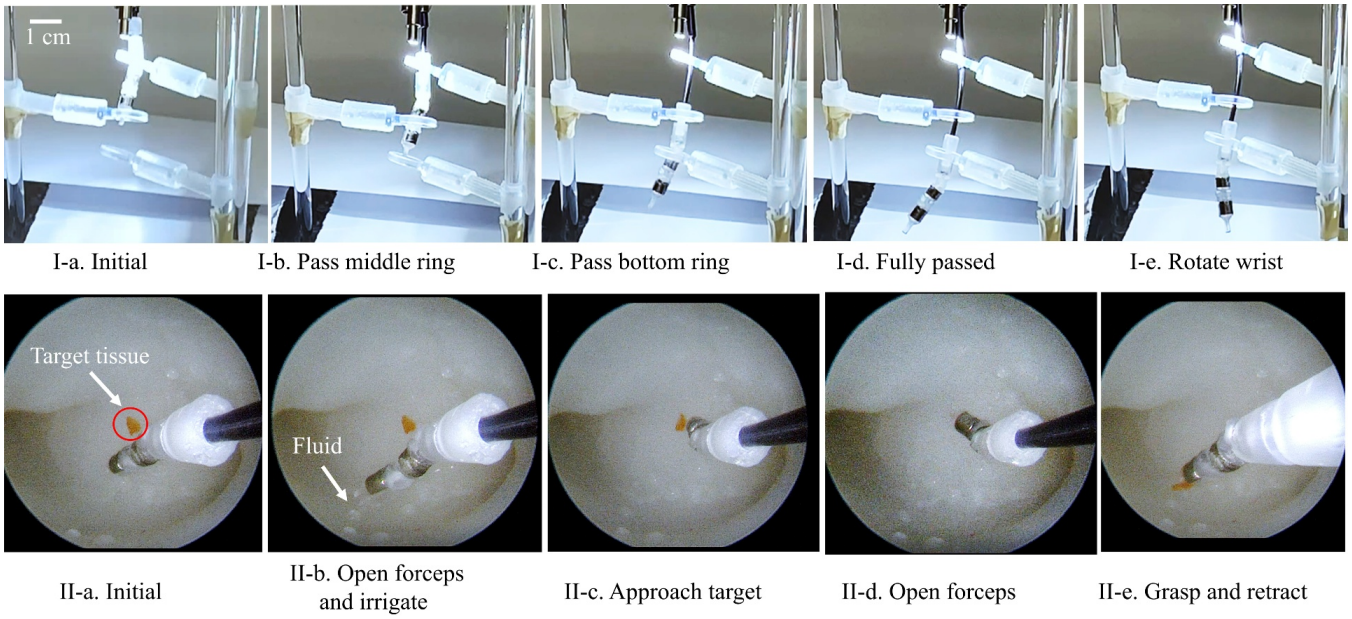

Fig. 8: Feasibility evaluation experiments. Top row: Hybrid robot is steered to pass through a set of three rings; Bottom row: Endoscopy view of mock diseased tissue removal by the hybrid robot.

forceps magnet m_2 to be parallel to the one of the wrist magnet m_1, which will be investigated in our future work.

The dynamics of the magnetic wristed forceps, including the forceps's gripping force and wrist's output torque are not focused on in this preliminary study, which is one of our future works. However, our previous research showed that the magnetic forceps could generate up to a 187 mN pushing force and a 83 mN gripping force [18], which are sufficient for a majority of epilepsy procedures. Due to limited choices for the off-the-shelf half-cylinder magnets, the magnetic wristed forceps is fabricated with a relatively large size compared to the CTR's tubes. In our future work, customized small magnets will be investigated to scale down the magnetic wrist and forceps.

Utilizing the wireless remote actuation with the magnetic field significantly simplified the transmission structure for the wristed forceps, which is typically actuated by sophisticated deployments of a set of cables in other wristed robotic tool designs. The use of 3D printed parts and low-cost off-the-shelf magnets can make the magnetic wristed forceps disposable. The downside of this hybrid approach is that a field source is needed in addition to the CTR drive system. However, eMNSs have already been used for a few pre-clinical procedures [23] and therefore our system could be deployed in an operating room without significantly changing the room's environment.

In the current implementation of the magnetic wristed tool, we used off-the-shelf ring magnets that have limited selection and resulted in the diameter of the tool shaft as 4 mm, which is somehow thick for micro-operations inside of the brain. However, the tool can be miniaturized by using customized magnets that have smaller diameters.

The results of this research will have a significant impact on epilepsy surgery by showing the feasibility of using steerable robotic tools to provide treatments while minimizing the trauma on the patient. The concept of steerable robotic tools will become a platform for a variety of different procedures. The platform can also be applied to other neurological conditions such as brain tumors, deep brain stimulation and targeted drug delivery. Surgeons will be able to plan complex treatments without the need for a larger invasive and traumatic exposure of the brain. Based on the historical impacts of laparoscopy on general surgery and urology, we expect patients to recover faster, hospitals to see reduced post-operative recovery costs, and to increase the frequency/access to treatment.

This preliminary study presented a hybrid robotic system that integrates a CTR and magnetically actuated wristed forceps. The design, modelling, and control of the hybrid system are introduced. The feasibility of applying the hybrid robot for epilepsy procedures is evaluated by performing phantom experiments. The results show that the hybrid robot is able to grasp the target tissue in a narrow space. Such technological advancements may allow technically difficult procedures to be performed in the microsurgical environment.

REFERENCES

[1] N. Hitiris, R. Mohanraj, J. Norrie, G. J. Sills, and M. J. Brodie, "Predictors of pharmacoresistant epilepsy," *Epilepsy research*, vol. 75, no. 2-3, pp. 192–196, 2007.

[2] S. Sgouros, "Neuroendoscopy: current status and future trends," 2013.

[3] C. Faria, W. Erlhagen, M. Rito, E. De Momi, G. Ferrigno, and E. Bicho, "Review of robotic technology for stereotactic neurosurgery," *IEEE Reviews in Biomedical Engineering*, vol. 8, pp. 125–137, 2015.

[4] Y. S. Kwoh, J. Hou, E. A. Jonckheere, and S. Hayati, "A robot with improved absolute positioning accuracy for ct guided stereotactic brain surgery," *IEEE transactions on biomedical engineering*, vol. 35, no. 2, pp. 153–160, 1988.

[5] M. J. Lang, A. D. Greer, and G. R. Sutherland, "Intra-operative robotics: Neuroarm," in *Intraoperative Imaging*. Springer, 2011, pp. 231–236.

[6] B. Davies, S. Starkie, S. Harris, E. Agterhuis, V. Paul, and L. Auer, "Neurobot: a special-purpose robot for neurosurgery," in *Proceedings 2000 ICRA. Millennium Conference. IEEE International Conference on Robotics and Automation. Symposia Proceedings (Cat. No.00CH37065)*, vol. 4, 2000, pp. 4103–4108 vol.4.

[7] M. Niccolini, V. Castelli, C. Diversi, B. Kang, F. Mussa, and E. Sinibaldi, "Development and preliminary assessment of a robotic platform for neuroendoscopy based on a lightweight robot," *The International Journal of Medical Robotics and Computer Assisted Surgery*, vol. 12, no. 1, pp. 4–17, 2016.

[8] C. J. Nycz, R. Gondokaryono, P. Carvalho, N. Patel, M. Wartenberg, J. G. Pilitsis, and G. S. Fischer, "Mechanical validation of an mri compatible stereotactic neurosurgery robot in preparation for preclinical trials," in *2017 IEEE/RSJ International Conference on Intelligent Robots and Systems (IROS)*. IEEE, 2017, pp. 1677–1684.

[9] C. Teo, S. Rahman, F. A. Boop, and B. Cherny, "Complications of endoscopic neurosurgery," *Child's Nervous System*, vol. 12, no. 5, pp. 248–253, 1996.

[10] H. J. Marcus, A. Hughes-Hallett, T. P. Cundy, G.-Z. Yang, A. Darzi, and D. Nandi, "da vinci robot-assisted keyhole neurosurgery: a cadaver study on feasibility and safety," *Neurosurgical review*, vol. 38, no. 2, pp. 367–371, 2015.

[11] A. Hong, A. J. Petruska, A. Zemmar, and B. J. Nelson, "Magnetic control of a flexible needle in neurosurgery," *IEEE Transactions on Biomedical Engineering*, vol. 68, no. 2, pp. 616–627, 2020.

[12] Y. Kim, E. Genevriere, P. Harker, J. Choe, M. Balicki, R. W. Regenhardt, J. E. Vranic, A. A. Dmytriw, A. B. Patel, and X. Zhao, "Telerobotic neurovascular interventions with magnetic manipulation," *Science Robotics*, vol. 7, no. 65, p. eabg9907, 2022.

[13] T. Gopesh, J. H. Wen, D. Santiago-Dieppa, B. Yan, J. S. Pannell, A. Khalessi, A. Norbash, and J. Friend, "Soft robotic steerable microcatheter for the endovascular treatment of cerebral disorders," *Science robotics*, vol. 6, no. 57, p. eabf0601, 2021.

[14] M. F. Rox, D. S. Ropella, R. J. Hendrick, E. Blum, R. P. Naftel, H. C. Bow, S. D. Herrell, K. D. Weaver, L. B. Chambless, and R. J. Webster III, "Mechatronic design of a two-arm concentric tube robot system for rigid neuroendoscopy," *IEEE/ASME Transactions on Mechatronics*, vol. 25, no. 3, pp. 1432–1443, 2020.

[15] J. Burgner, D. C. Rucker, H. B. Gilbert, P. J. Swaney, P. T. Russell, K. D. Weaver, and R. J. Webster, "A telerobotic system for transnasal surgery," *IEEE/ASME Transactions on Mechatronics*, vol. 19, no. 3, pp. 996–1006, 2014.

[16] P. E. Dupont, J. Lock, B. Itkowitz, and E. Butler, "Design and control of concentric-tube robots," *IEEE Transactions on Robotics*, vol. 26, no. 2, pp. 209–225, 2009.

[17] R. J. Webster, A. M. Okamura, and N. J. Cowan, "Toward active cannulas: Miniature snake-like surgical robots," in *2006 IEEE/RSJ international conference on intelligent robots and systems*. IEEE, 2006, pp. 2857–2863.

[18] A. Lim, A. Schonewille, C. Forbrigger, T. Looi, J. Drake, and E. Diller, "Design and comparison of magnetically-actuated dexterous forceps instruments for neuroendoscopy," *IEEE Transactions on Biomedical Engineering*, vol. 68, no. 3, pp. 846–856, 2021.

[19] P. Dupont, N. Simaan, H. Choset, and C. Rucker, "Continuum robots for medical interventions," *Proceedings of the IEEE*, 2022.

[20] P. Sears and P. E. Dupont, "Inverse kinematics of concentric tube steerable needles," in *Proceedings 2007 IEEE international conference on robotics and automation*. IEEE, 2007, pp. 1887–1892.

[21] A. Schonewille, "Maximizing workspace accessibility in magnetic actuation of tethered microsurgical tools using non-uniform magnetic fields," Master's thesis, University of Toronto, Canada, 2022.

[22] G. E. Breimer, V. Bodani, T. Looi, and J. M. Drake, "Design and evaluation of a new synthetic brain simulator for endoscopic third ventriculostomy," *Journal of Neurosurgery: Pediatrics*, vol. 15, no. 1, pp. 82–88, 2015.

[23] S. Gervasoni, J. Lussi, S. Viviani, Q. Boehler, N. Ochsenbein, U. Moehrlen, and B. J. Nelson, "Magnetically assisted robotic fetal surgery for the treatment of spina bifida," *IEEE Transactions on Medical Robotics and Bionics*, vol. 4, no. 1, pp. 85–93, 2022.